



Contents lists available at ScienceDirect

## Journal of Non-Newtonian Fluid Mechanics

journal homepage: [www.elsevier.com/locate/jnnfm](http://www.elsevier.com/locate/jnnfm)



# What is the final shape of a viscoplastic slump?

N. Dubash<sup>a,\*</sup>, N.J. Balmforth<sup>a,b</sup>, A.C. Slim<sup>a</sup>, S. Cochard<sup>a</sup>

<sup>a</sup> Department of Mathematics, University of British Columbia, Vancouver, Canada

<sup>b</sup> Department of Earth and Ocean Science, University of British Columbia, Vancouver, Canada

### ARTICLE INFO

#### Article history:

Received 14 April 2008

Received in revised form 4 August 2008

Accepted 14 August 2008

Available online xxx

#### Keywords:

Viscoplastic fluids

Yield stress

Deposit shape

### ABSTRACT

The final shape of a two-dimensional viscoplastic slump is constructed assuming that the fluid yielded everywhere in its passage to the final state and that the yield stress dominates except in a viscous boundary layer at the base. These assumptions reduce the problem to a related one in plasticity theory. Two methods are presented. First, an asymptotic expansion based on small aspect ratio,  $\epsilon$ , is used to build an analytical solution valid to third order in  $\epsilon$ . Second, a slipline method is used to construct slump shapes for arbitrary aspect ratio. The slipline theory exposes flaws in the assumption that the fluid yields everywhere, and rigid plug zones must be inserted in the solution to match all the boundary conditions. The results are compared to a set of experiments with Carbopol in which fluid slumps down a channel. Care is taken to ensure that the width of the channel, any slip over the walls, and the mechanism of emplacement are not important. Despite this, the experiments and theory are not in particularly good agreement, suggesting that some of the theoretical assumptions are invalid.

© 2008 Elsevier B.V. All rights reserved.

## 1. Introduction

A large number of industrial and geophysical problems involve the spreading of viscoplastic fluids under gravity over horizontal and inclined surfaces. Unlike viscous fluids, which continue to flow until restricted by physical obstructions or surface tension, viscoplastics can come to rest under the action of the yield stress. In fact, in certain rheological tests, the resting shape of a slumped viscoplastic fluid is used to infer the yield stress. This “slump test” is widely used to gauge the yield strength of concrete [1–3], and has been used for a variety of other industrial and geophysical materials [4–6].

In the current paper we examine the final shape for a two-dimensional deposit of viscoplastic fluid on an inclined surface. Such a situation is relevant for flow along an infinitely wide channel, and could be the result of a slump, a dam break, or an extrusion from a vent. But for a single exception, all previous theoretical work on this problem that attempted to construct explicitly the final shape has been carried out using a simplifying shallow-layer approximation, which is appropriate when the yield stress is relatively small [7]. The exceptional study is by Nye [8], who built a slump shape as a model of a glacier, assuming that ice behaved like a slowly moving, perfectly plastic material and using the slipline method of plasticity

theory [9,10]. Nye’s solution is relevant to the current viscoplastic problem because, in the zero-shear-rate limit, a viscoplastic fluid is controlled predominantly by its yield stress and the constitutive law then reduces to that for a perfect plastic. Moreover, Nye’s plastic glacier slides over a lubricating layer at its base, and the stresses are locally dominated by the shear stress; this situation is mirrored by a viscoplastic fluid as it brakes to rest because the bulk of the fluid most likely rides over a viscous boundary layer adjacent to the underlying plane [11].

In the current study we extend the known theoretical results in two ways. First, we continue to higher order in the aspect ratio the asymptotic expansion whose leading order provides the standard shallow-layer approximation. This provides a more accurate analytical formula for the slump profile as one advances away from the shallow limit. Second, we reformulate Nye’s analysis for the current problem, giving a solution valid for any aspect ratio. As we shall see, Nye’s solution is the natural extension of the shallow-layer theory. However, it also turns out that, in order to satisfy all the boundary conditions, some rigid plug zones must be inserted into the slipline solution.

To compare with the theoretical prediction, we also conduct a suite of simple experiments using Carbopol (Ultrez 10 & 21). This proto-typical viscoplastic material was previously used by Cochard [12] in dambreak experiments down an inclinable channel (see also [13]), and we use some of the data reported there in our comparisons. The current experiments extend Cochard’s results by varying the channel’s width and the mechanism by which the fluid is released, all to gauge the effect of the correspond-

\* Corresponding author at: Department of Mathematics, University of British Columbia, 1984 Mathematics Road, Vancouver, Canada V6T 1Z2  
E-mail address: [ndubash@math.ubc.ca](mailto:ndubash@math.ubc.ca) (N. Dubash).

ing physical effects (side-wall resistance and the emplacement mechanism).

The outline of the paper is as follows. In Section 2 we present the governing equations. Section 3 contains the shallow-layer perturbation analysis. The slipline theory construction for non-shallow slumps is presented in Section 4. In Section 5 the results of the two different theories are examined and compared, and Section 6 contains the experimental results. Section 7 draws our conclusions. The appendices contain technical details of the asymptotic and slipline analysis.

## 2. Problem formulation

### 2.1. Dimensional equations

The momentum equations for a deposit of viscoplastic material on a plane inclined at an angle  $\phi$  to the horizontal are

$$-\frac{\partial \hat{p}}{\partial \hat{x}} + \frac{\partial \hat{\tau}_{xx}}{\partial \hat{x}} + \frac{\partial \hat{\tau}_{xz}}{\partial \hat{z}} + \rho g \sin \phi = 0, \quad (1)$$

$$-\frac{\partial \hat{p}}{\partial \hat{z}} + \frac{\partial \hat{\tau}_{xz}}{\partial \hat{x}} + \frac{\partial \hat{\tau}_{zz}}{\partial \hat{z}} - \rho g \cos \phi = 0, \quad (2)$$

where  $\hat{p}$  is the pressure,  $\hat{\tau}_{ij}$  is the deviatoric stress tensor,  $\rho$  is the density, and  $g$  is the gravitational acceleration. The coordinates  $\hat{x}$  and  $\hat{z}$  are orientated along and perpendicular to the inclined plane, respectively. (The hats are added to distinguish the dimensional variables we begin with from their dimensionless counterparts which appear below.)

The deviatoric stresses follow from a viscoplastic constitutive law which we assume to take the yielded form,

$$\hat{\tau}_{jk} = \left[ \frac{\tau_Y}{\dot{\gamma}} + \eta(\dot{\gamma}) \right] \dot{\gamma}_{jk}, \quad (3)$$

where  $\dot{\gamma}_{jk}$  denote the components of the deformation rate tensor,  $\dot{\gamma}_{jk} = \partial u_j / \partial \hat{x}_k + \partial u_k / \partial \hat{x}_j$ ,  $\dot{\gamma}$  is its second invariant and  $u_j$  denotes the components of the velocity field;  $\tau_Y$  is the yield stress and  $\eta$  is the viscosity. In the limit that deformation rates approach zero, the yield stress dominates and

$$\hat{\tau}_{jk} \rightarrow \frac{\tau_Y}{\dot{\gamma}} \dot{\gamma}_{jk}. \quad (4)$$

Thus,

$$\hat{\tau}_{xx}^2 + \hat{\tau}_{xz}^2 = \tau_Y^2, \quad (5)$$

if the fluid is incompressible, implying  $\hat{\tau}_{zz} = -\hat{\tau}_{xx}$ .

We assume that the fluid approaches its final state after yielding everywhere, so that (5) holds throughout the final deposit. Unfortunately, this assumption leads to an inconsistency since the stress field implied by (1) and (2) does not in general furnish velocity fields through (4) that satisfy the no-slip condition on the underlying plane. Guided by shallow-layer theory [11], we argue that the final sheared motion of the fluid actually takes place mainly in a viscous boundary layer adjacent to the underlying plane. In this boundary layer, the viscous terms cannot be neglected in comparison to the yield stress, and their reinstatement allows the velocity field to be corrected to accommodate the no-slip condition.

The principal effect of the viscous boundary layer on the stress field is to demand that shear stresses dominate the stress tensor as  $\hat{z} \rightarrow 0$ , leading to the basal boundary condition,

$$\hat{\tau}_{xz} \rightarrow \tau_Y, \quad \hat{\tau}_{xx} \rightarrow 0 \quad \text{for } \hat{z} \rightarrow 0. \quad (6)$$

Thus the problem reduces to Nye's plasticity problem in which a perfectly plastic material slides over a lubricated base.

The other boundary condition required is at the free surface, denoted by  $\hat{z} = \hat{h}(\hat{x})$ , where the force balance imposes

$$\begin{pmatrix} -\hat{p} + \hat{\tau}_{xx} & \hat{\tau}_{xz} \\ \hat{\tau}_{xz} & -\hat{p} - \hat{\tau}_{xx} \end{pmatrix} \begin{pmatrix} -\hat{h}_{\hat{x}} \\ 1 \end{pmatrix} = \begin{pmatrix} 0 \\ 0 \end{pmatrix}, \quad (7)$$

with  $\hat{h}_{\hat{x}} = \partial \hat{h} / \partial \hat{x}$ .

### 2.2. Dimensional considerations

The principal dimensional constants ( $g$ ,  $\rho$  and  $\tau_Y$ ) imply a characteristic lengthscale,

$$\ell = \frac{\tau_Y}{\rho g \cos \phi}. \quad (8)$$

Moreover, since there are only two dimensional constants with the units of space and time, one might therefore conclude that there are seemingly no free dimensionless parameters in the problem other than the inclination of the plane,  $\phi$ . The flaw in the argument is that the slump always begins with a fixed amount of material (expressed as an area,  $\mathcal{A}$ ), which is conserved throughout the subsequent motion. Thus, there is a second lengthscale,  $\sqrt{\mathcal{A}}$ , and another dimensionless parameter,  $\ell / \sqrt{\mathcal{A}}$ .

Nevertheless, our construction of the final shape proceeds without knowing the final area and ignores all the preceding dynamics, and so we have no way of connecting the solution with  $\sqrt{\mathcal{A}}$  a priori. To make matters worse, one of our goals is an asymptotic expansion based on the small aspect ratio of the final deposit. Hence the characteristic length and height of the final deposit are not even of the same order. In this situation, it is not convenient to use  $\sqrt{\mathcal{A}}$  as a characteristic lengthscale, and we must proceed slightly differently. Instead, we introduce a characteristic height scale for the final shape,  $H_{\text{char}}$ , and determine its relation with  $\sqrt{\mathcal{A}}$  a posteriori. Moreover, for the asymptotics and the slipline theory we choose  $H_{\text{char}}$  in two different ways in order to simplify the analyses; see Section 2.3.

Given the scale,  $H_{\text{char}}$  (which is indicated in Section 2.3), we now non-dimensionalize the equations: we scale heights ( $\hat{z}$  and  $\hat{h}$ ) and length ( $\hat{x}$ ) by  $H_{\text{char}}$  and  $\epsilon^{-1} H_{\text{char}}$ , respectively, where

$$\epsilon = \frac{\ell}{H_{\text{char}}} = \frac{\tau_Y}{\rho g H_{\text{char}} \cos \phi}. \quad (9)$$

Pressures are scaled with  $\rho g H_{\text{char}} \cos \phi$ , and stresses with  $\tau_Y$ . Eqs. (1)–(5) then become

$$-\frac{\partial p}{\partial x} + \epsilon \frac{\partial \tau_{xx}}{\partial x} + \frac{\partial \tau_{xz}}{\partial z} + S = 0, \quad (10)$$

$$-\frac{\partial p}{\partial z} + \epsilon^2 \frac{\partial \tau_{xz}}{\partial x} + \epsilon \frac{\partial \tau_{zz}}{\partial z} - 1 = 0, \quad (11)$$

$$\tau_{xx}^2 + \tau_{xz}^2 = 1, \quad (12)$$

where

$$S = \frac{1}{\epsilon} \tan \phi. \quad (13)$$

After a little algebra, and using the yield condition (12), the force balance conditions on the free surface can be written in the alternative, dimensionless form,

$$p = \epsilon, \quad \tau_{xx} = -\tau_{zz} = -\frac{(1 - \epsilon^2 h_x^2)}{1 + \epsilon^2 h_x^2},$$

$$\tau_{xz} = -\frac{2\epsilon h_x}{1 + \epsilon^2 h_x^2}, \quad \text{on } z = h. \quad (14)$$

Here, we have made the implicit assumption that the material has slumped to the right (the positive  $x$  direction) and that the

material surface is in compression, so that  $u_x < 0$  and  $\tau_{xx} < 0$  on  $z = h$ . The basal boundary condition becomes

$$\tau_{xz} = 1, \quad \tau_{xx} = 0 \quad \text{on } z = 0. \quad (15)$$

### 2.3. Scaling issues

The preceding dimensionless formulation contains an arbitrary characteristic height scale,  $H_{\text{char}}$ . This scale can be selected in order to simplify the asymptotic analysis and the slipline theory. However, the choices are different, which forces us to connect explicitly the two formulations after describing each separately.

More specifically, the asymptotic analysis (Section 3) is expedited if we choose  $H_{\text{char}}$  as the maximum height of the final deposit, and then demand  $\epsilon \ll 1$  for the effective aspect ratio,  $\epsilon$ . The connection of the analysis with a small-yield-stress theory is then clear from the definition of that parameter.

The numerical computation of the slipline theory (Section 4), on the other hand, proceeds far more simply if we choose  $\epsilon = 1$ . That is, we use  $\hat{\ell}$  to scale all lengths and heights. This leaves an apparently parameterless problem in (10)–(15) with a unique solution for each value of  $\phi$ . This “master profile” has no maximal height specified, and one ends the calculation by truncating the profile and thereby identifying this parameter. How the truncation relates to the actual boundary conditions will also be given in Section 4.

The truncation furnishes both the maximum dimensionless height and also the length of the deposit,  $L_M \equiv f(H_M; \phi)$ . In dimensional terms, one may then write,

$$\hat{L} = \ell f\left(\frac{\hat{H}}{\ell}; \phi\right), \quad (16)$$

where  $\hat{L}$  and  $\hat{H}$  are the dimensional length and height. Now, if we instead choose  $\hat{H}$  to scale lengths, then

$$L = \frac{\hat{L}}{\hat{H}} = Bf(B^{-1}; \phi), \quad (17)$$

where

$$B \equiv \frac{\ell}{\hat{H}} = \frac{\tau_Y}{\rho g \hat{H} \cos \phi}, \quad (18)$$

is an equivalent yield-stress parameter, or Bingham number. For example, to find the length of the slump for  $B = 0.5$  we simply evaluate the length of the master profile at  $H_M = B^{-1} = 2$  and then multiply that length by a factor of 0.5. Note that  $B \rightarrow \epsilon \ll 1$  for the asymptotics, and therefore our rescaled problem corresponds to that theory in the small aspect ratio limit. However, lengths in  $x$  are scaled with an additional factor of  $\epsilon^{-1}$  in the asymptotic analysis.

### 3. Shallow-layer theory

For shallow slumps where  $\epsilon \ll 1$ , the profiles may be calculated using a perturbation expansion. We further assume shallow inclines with  $\tan \phi = O(\epsilon)$  and thus  $S = O(1)$ . The details of these calculations are given in Appendix A, and we quote only the main results here.

For a horizontal surface ( $S = 0$ ), we obtain

$$h = \sqrt{\left(1 + \frac{\pi}{2}\epsilon\right)^2 - 2x - \frac{\pi}{2}\epsilon + O(\epsilon^3)}. \quad (19)$$

The corresponding slump length is then given by

$$L = \frac{1}{2} + \frac{\pi}{2}\epsilon + O(\epsilon^3). \quad (20)$$

The leading (zeroth-)order parabolic profile, given by  $\epsilon = 0$ , was previously obtained by Nye [14]. Later, Nye [8] also reported the

first-order correction term to (20), although it was derived through a more heuristic argument. As we see in (20), Nye’s correction is actually accurate to order  $\epsilon^3$ .

For an inclined surface ( $S \neq 0$ ), we write the solution for the profile implicitly as

$$h - 1 + \left[\frac{1}{S} + \epsilon\frac{\pi}{2} + \epsilon^2\left(3 - \frac{\pi^2}{4}\right)S\right] \log\left(\frac{1 - Sh}{1 - S}\right) + O(\epsilon^3) = Sx. \quad (21)$$

Such solutions only exist for  $S < 1$ , which reflects the general result that the yield stress can only hold the fluid layer on the slope provided that the depth is not too large. The slump length is

$$L = -\frac{1}{S} - \frac{1}{S^2} \log(1 - S) - \epsilon\frac{\pi}{2S} \log(1 - S) - \epsilon^2\left(3 - \frac{\pi^2}{4}\right) \log(1 - S) + O(\epsilon^3). \quad (22)$$

Again, the leading order terms in (21) and (22), have been derived previously [6,14,15].

## 4. The master profile

### 4.1. Slipline theory

We now consider the Eqs. (10)–(15) with  $\epsilon = 1$ . In addition we introduce a new variable,

$$P = p + z - xS, \quad (23)$$

which represents the (non-dimensional) pressure with the hydrostatic component extracted. Thus (10) and (11) become

$$-\frac{\partial P}{\partial x} + \frac{\partial \tau_{xx}}{\partial x} + \frac{\partial \tau_{xz}}{\partial z} = 0, \quad (24)$$

$$-\frac{\partial P}{\partial z} + \frac{\partial \tau_{xz}}{\partial x} + \frac{\partial \tau_{zz}}{\partial z} = 0, \quad (25)$$

and the first equation of (14) becomes

$$P - h + xS - 1 = 0 \quad \text{on } z = h. \quad (26)$$

Following standard plasticity theory we introduce a set of orthogonal characteristic curves or sliplines, denoted by  $\alpha$  and  $\beta$  [9,10]. (For the two-dimensional problem the sliplines and the characteristics are the same.) These sliplines are orientated such that the direction of the algebraically greatest principal stress bisects the angle between the  $\alpha$ - and  $\beta$ -characteristics. (The sliplines are orientated in the directions of maximum shear stress.) If  $\theta$  is the counterclockwise angle the  $\alpha$ -characteristic makes with the  $x$  axis, we write

$$\tau_{xx} = -\tau_{zz} = -\sin 2\theta, \quad \tau_{xz} = \cos 2\theta. \quad (27)$$

Along the characteristic curves the following quantities are conserved [9,10]:

$$P + 2\theta = \text{constant} \quad \text{along an } \alpha\text{-characteristic, and} \quad (28)$$

$$P - 2\theta = \text{constant} \quad \text{along a } \beta\text{-characteristic.} \quad (29)$$

From Eq. (14) we can write

$$h_x^2 - 2h_x \tan 2\theta - 1 = 0, \quad \text{on } z = h. \quad (30)$$

After some algebra this can be factored to obtain

$$\tan(\tan^{-1} h_x - \theta) = \pm 1 \quad \text{on } z = h. \quad (31)$$



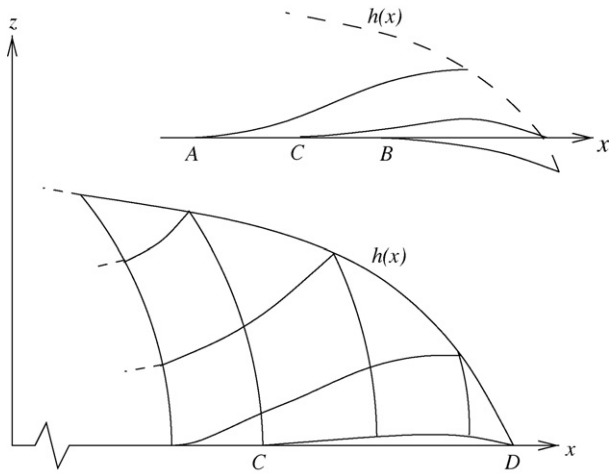


Fig. 3. A diagram of the slipline field near the end of the profile.

this curve. Because any of the characteristic curves can be considered to be a yield surface, the fluid sandwiched between the last  $\alpha$ -characteristic and the base can be considered to be a rigid plug. Whether this is compatible with the idea of an underlying viscous boundary layer is not clear. In practice though, this plug on the base is very small.

Finally, to determine a profile for a slump with maximal height  $\hat{H}$ , we truncate the master profile at the height  $h = \hat{H}/\ell = B^{-1}$ , as in Eq. (18). Provided that  $B^{-1}$  is sufficiently smaller than  $H_*$ , the effects of the initial expansion fan and  $\alpha_0$  are thereby removed, leaving a master profile beginning on the left with a distinguished  $\beta$ -characteristic; see Fig. 4. Again, the wedge of material to the left of that  $\beta$ -characteristic can be taken to be a rigid plug. In this way, we can join the solution onto a stagnant wedge abutting a back wall, an upstream layer of unyielded fluid, or a unyielded core separating deposits that slumped in either direction (see Fig. 4). The relevant upstream boundary conditions are thereby taken care of, if at the expense of the introduction of a rigid plug.

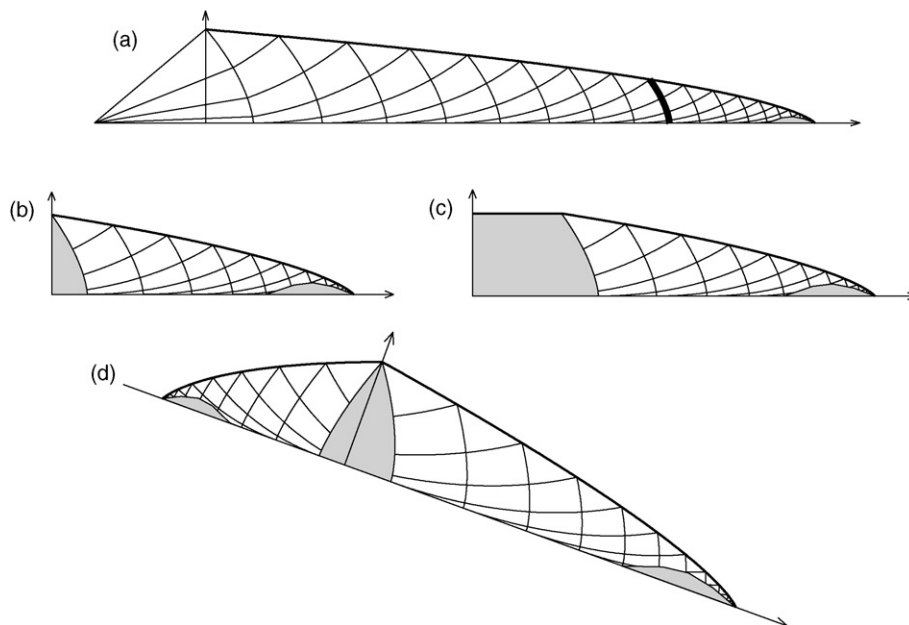


Fig. 4. (a) The slipline construction is truncated along a  $\beta$ -characteristic sufficiently far from the initial expansion fan (on the left). The resulting solution can then be joined to (b) a stagnant wedge abutting a back wall, (c) an upstream layer of unyielded fluid, or (d) an unyielded core separating deposits slumped in either direction. Note that the unyielded regions near the front of the slumps have been exaggerated for visibility.

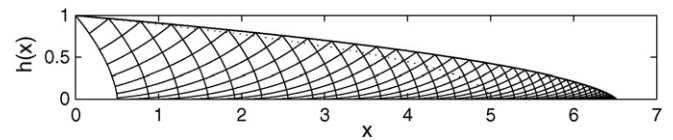


Fig. 5. The surface profile and slipline field for a slump with  $B = 0.1$  and  $\phi = 0$ . The dotted line is the leading order shallow-layer profile (the second-order solution is indistinguishable from the slipline profile).

## 5. Results

Typical slipline fields and surface profiles are shown in Figs. 5 and 6 for  $B = 0.1$  and  $0.8$ , respectively (and  $\phi = 0$ ). Fig. 6 b shows the detail of the slipline field near the end of the profile. Note that only a fraction of the calculated sliplines are shown, in order to avoid cluttering the figures. Also shown in Figs. 5 and 6 are the shallow-layer profiles predicted by Eq. (19), (the leading order solution  $h = \sqrt{1 - 2x}$ , as well as the second-order solution). Fig. 7 compares slump profiles from the slipline theory with those from the shallow-layer theory (Eq. (21)), for different inclination angles and for different values of  $B$ . (In these cases the leading order approximation is much more inferior and is omitted for clarity.) Note that the cases with  $\phi < 0$  correspond to slumps upslope.

Fig. 8 shows the length,  $L$ , of the deposit for  $\phi = 0$  as a function of  $B$ . The asymptotic analysis (with small  $B \equiv \epsilon$ ) predicts the length,

$$L = \frac{1}{2B} + \frac{\pi}{2}. \quad (35)$$

(Recall that in Section 3 lengths are scaled with additional factor of  $\epsilon^{-1}$ .) Using a force balance argument over the entire profile (including the initial expansion fan), Nye [8] derived the alternative,

$$L = \frac{1}{2B} + 1. \quad (36)$$

Both predictions (35) and (36) are included in Fig. 8. Unsurprisingly, while both predictions match the general trend of the data (Fig. 8, inset), the asymptotics are more accurate for small  $B$ , because (36) incorporates the effect of the initial expansion fan. As pointed

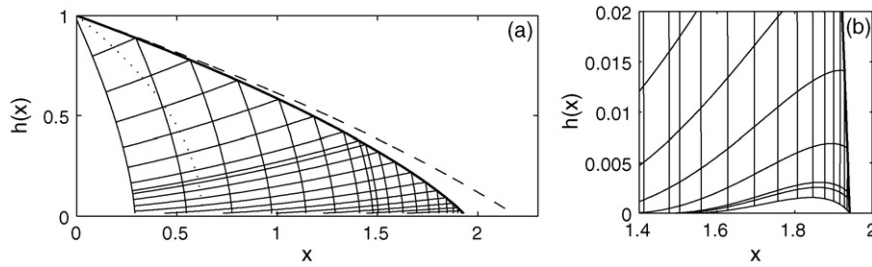


**Fig. 6.** (a) The surface profile and slipline field for a slump with  $B = 0.8$  and  $\phi = 0$ . The dotted and dashed lines are, respectively, the leading order and second-order shallow-layer profile given by Eq. (19). (b) Detail of slipline field near the end of the profile. Here no new  $\alpha$ -characteristics are being generated.

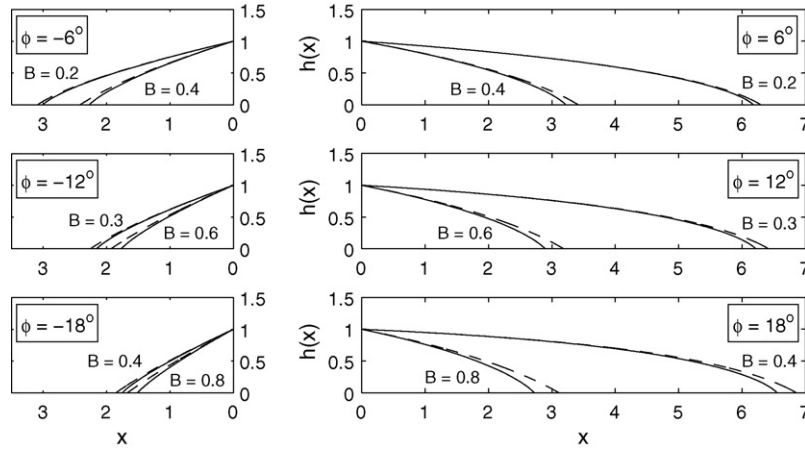


**Fig. 7.** Slump profiles given by the slipline theory (solid lines) and by the shallow-layer theory (second-order solution, dashed lines) for various values of  $\phi$  and  $B$ .

out by Nye, in his force balance the pressure is assumed to be linear at the left edge, which is not the case even for shallow slumps.

Fig. 9 shows the slump length as a function of  $B$  for different inclination angles. As noted before, for  $\phi \neq 0$ , there is a critical layer height above which the deposit cannot be held on the slope by the yield stress. After rescaling the master profile as in Section 2.3, so that the height is unity, this limit translates to a lower bound on  $B$  which must be exceeded for the slump to become static. The relevant critical values of  $B$  are also shown in Fig. 9. Because we have imposed that the fluid must slump to the right, we can in practice obtain slump profiles for arbitrarily small  $B$  when  $\phi < 0$ .

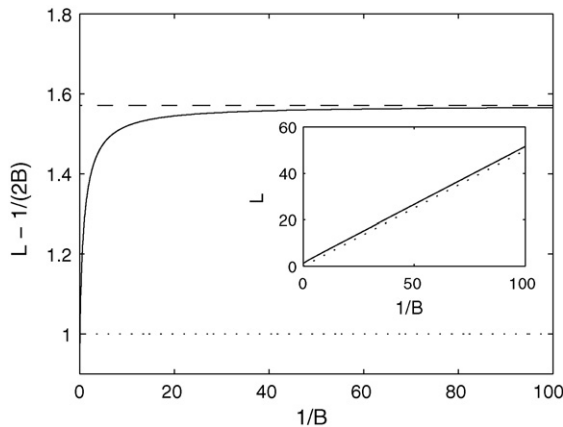


**Fig. 8.** The behaviour of the slump length,  $L$ , as a function of  $B$  from the slipline theory (solid line) and the shallow-layer theory (dashed line);  $\phi = 0$ . Also shown is Eq. (36) for Nye's force balance (dotted line). The inset shows the general trend for  $L$ ; the dotted line represents a slope of  $1/2$ .

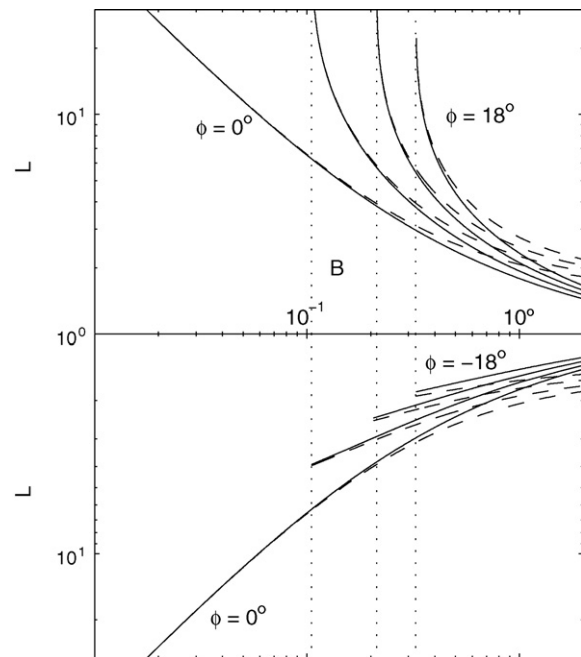


**Fig. 9.** The behaviour of the slump length,  $L$ , as a function of  $B$ , for  $\phi = 0^\circ, 6^\circ, 12^\circ$ , and  $18^\circ$  (upper panel,  $\phi$  increasing from left to right) and  $\phi = -18^\circ, -12^\circ, -6^\circ$ , and  $0^\circ$  (lower panel,  $\phi$  increasing from top to bottom). The solid lines represent the slipline theory, the dashed lines represent the shallow-layer theory, and the dotted lines represent the critical  $B$  values required for a static slump to exist.

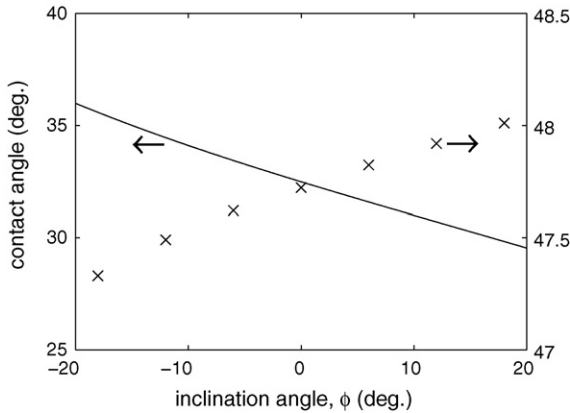


**Fig. 10.** The contact angle (relative to the inclined surface) plotted versus the angle of inclination,  $\phi$ , from the asymptotic analysis (solid line, left axis scale), and the slipline theory ( $\times$ , right axis scale).

However, physically, these uphill slumps are also restricted by the lower bound in  $B$ , as otherwise they cannot hold themselves up against collapsing to the left (i.e., downhill).

In both the slipline theory and the asymptotics, the angle of the surface at the edge of the deposit (the “contact angle”) is finite and independent of  $B$ . For  $\phi = 0$ , the slipline theory predicts a contact angle of about  $47.72^\circ$ , as also mentioned by Nye. The corresponding asymptotic result is  $\tan^{-1}(2/\pi) \approx 32.48^\circ$ . These values vary weakly with the slope (see Fig. 10). In the slipline theory the contact angle is directly calculated in the construction, and in the asymptotics the contact angle is determined by differentiation of (19) and (21). Physically, one expects the contact angle to increase with  $\phi$ , which is the trend given by the slipline analysis. The asymptotics, on the other hand, show the opposite; however, here the analysis breaks down as we approach the front of the slump, so the angle predictions should be considered less than trustworthy.

## 6. Experiments

The majority of existing experimental work on the final shape of slumped deposits is either axisymmetric or fully 3D. And most of the reported experiments carried out in channels [16] either do not fully come to rest, or are overly affected by either inertia or the side-walls. Thus, in order to compare our theory with observations, we conducted our own experiments with Carbopol in a horizontal glass tank 100 cm long, 30 cm wide, and 16 cm high. The base of the tank was covered by a thin textured foam sheet in order to prevent slip which is a known problem with Carbopol.<sup>1</sup> Slip was observed to occur along the side and back walls of the tank. However, as the primary purpose of the experiments was to test the two-dimensional theory, we considered the slip along the walls to be beneficial. The majority of the experiments were done with the full channel width, 30 cm, however some addition experiments were done in narrower channels (10 cm, 20 cm) to gauge the extent of the wall effects. It was found that for the 30 cm wide channel the wall effects were negligible (at least as far as the centre-line profile was concerned). In fact, wall effects only became noticeable when the channel width was reduced to 10 cm, and then only for the largest volume slumps with the smallest yield stress fluid.

<sup>1</sup> An experiment was also done where the base was covered with waterproof sandpaper (P220 ISO grit) and the result was identical to that with the textured foam sheet.

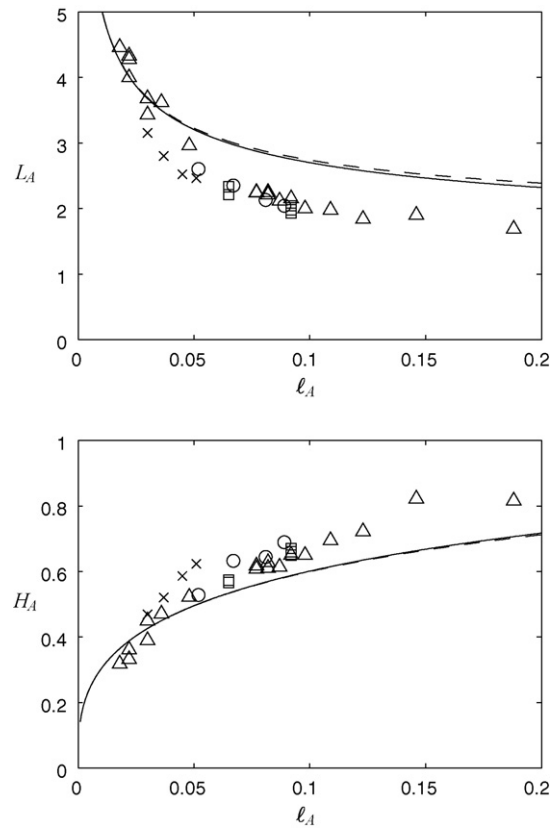


**Fig. 11.** Experimental results: our experiments,  $\Delta$  (tilted) and  $\square$  (gate); data from Cochard,  $\circ$  and  $\times$  (wall effect). Also shown are the results for the shallow-layer theory (dashed line) and the slipline theory (solid line).

Two different Carbopol solutions were used. The solutions were prepared according to the method described in [12]. The first was a 0.15 wt.% solution of Carbopol Ultrez 21, which had a yield stress of  $30 \pm 2$  Pa; the second was a 0.30 wt.% solution of Carbopol Ultrez 10, which had a yield stress of  $91 \pm 2$  Pa. The yield stress was measured using successive creep tests in a Bohlin rotational rheometer with a serrated plate–plate configuration. A range of different initial fluid areas  $\mathcal{A}$  (i.e., volumes) were used—from  $24 \text{ cm}^2$  up to  $300 \text{ cm}^2$ .

The experimental data is non-dimensionalized using  $\sqrt{\mathcal{A}}$ , thus the quantities of interest are

$$\ell_A = \frac{\ell}{\sqrt{\mathcal{A}}} = \frac{\tau_Y}{\rho g \sqrt{\mathcal{A}}}, \quad L_A = \frac{\hat{L}}{\sqrt{\mathcal{A}}}, \quad H_A = \frac{\hat{H}}{\sqrt{\mathcal{A}}}. \quad (37)$$

To begin with, the fluid was released by quickly raising a gate in the tank, in the manner of a conventional dambreak experiment. However, this release mechanism would always leave an impression along the free surface (in the form of a sharp ridge across the entire surface), and for the smaller values of  $\mathcal{A}$  the size of the ridge would become comparable to  $\hat{H}$ . In order to avoid the gate effect, we chose instead to tilt the tank backwards and emplace a triangular wedge of fluid of the desired volume. The tank was then slowly tilted back to the horizontal position. In all cases, all of the “released” material flowed.

Our theory only builds the final resting shape, and the basic assumption is that this shape is independent of the passage to the final state. Thus, different initial conditions should lead to the same final profile.

Experimental data for the scaled final lengths and heights are shown in Fig. 11. The different data all appear to collapse onto the same curve, indicating that the various release mechanisms did not

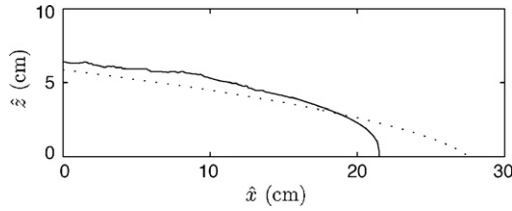


**Fig. 12.** Slump profile from an experiment (solid line) compared with the profile predicted by the slipline theory (dotted line). (The slipline profile and the shallow-layer profile are in such close agreement in this case that the latter has been omitted for clarity.) The experiment was with Carbopol Ultrez 10 with a yield stress of 91 Pa, and an initial volume corresponding to  $\mathcal{A} = 100 \text{ cm}^2$ . Note also that the contact angle is much larger than that predicted by the theory.

have a significant effect on the recorded final lengths and heights. We have also included some experimental results from Cochard [12] for dam breaks using Carbopol solutions in a channel. Note that we believe that some of Cochard’s data (those denoted by  $\times$ ) exhibit some wall effects resulting in larger  $H_A$  and smaller  $L_A$  values. For small values of  $\ell_A$  (the small-yield-stress limit), the experiments and the theory agree. However, for larger values of  $\ell_A$  there is a noticeable discrepancy—the theory predicting longer profiles than actually obtained. We have yet to come up with a satisfactory explanation of this. Fig. 12 shows the slump profile from an experiment compared with the theoretical profile. The discrepancy is clearly visible in this case (here  $\ell_A = 0.092$ ). Of further concern is that the contact angle in the experiments were all closer to  $90^\circ$  rather than the predicted  $47.7^\circ$  (see Fig. 12).

The discrepancy between the experiments and the theory indicate that some of the theoretical assumptions may be invalid, or that there are other physical effects which need to be accounted for. For example, surface tension could have an appreciable influence on the slump shape. Also, Carbopol has been observed to have some elastic effects at low stresses. One would expect that both surface tension and elastic effects would result in shorter slumps. Furthermore, a practical concern with the experiments is when can a slump be considered to have come to rest. In our experiments the final profile was measured once the front velocity had decreased to below 1 mm/h (usually about 3–6 h). However, in a careful experiment, Cochard [12] showed that the front could continue to move for up to 40 h (albeit at velocities much smaller than 1 mm/h) at which point evaporation of the fluid became a concern. In order to determine the source of the discrepancy, these issues will need to be examined in more detail.

## 7. Concluding remarks

In this article we have built the final shape of a viscoplastic slump using two methods: an asymptotic expansion for small  $B$ , and a slipline computation for arbitrary  $B$ , where  $B$  is an effective aspect ratio, or equivalently, a dimensionless yield stress. A notable feature of the equations is that if we do not impose the maximal height of the slump (or the total volume per unit width), then the governing equations (scaled with  $\ell$  as the length scale) are invariant under the transformation  $(x, z, h, p, \tau_{ij}, B) \rightarrow (\lambda x, \lambda z, \lambda h, \lambda p, \lambda \tau_{ij}, \lambda B)$ ; i.e., magnifying a slump profile for a Bingham number  $B$  by a factor of  $\lambda$  results in a solution for the system with Bingham number  $\lambda B$ . Unfortunately, to initiate the slipline construction a maximal height must be imposed. Nonetheless, it is the above invariance that allows the construction of the master profile (for a sufficiently large maximal height). The slipline theory also requires the inclusion of a rigid plug region near the slump tip. The compatibility of this with the viscous boundary layer can not be determined from the present analyses, and further work will be

necessary to resolve this matter. We are in the process of conducting detailed numerical simulations of the problem which we hope will clarify the matter; the results of which will be presented in a future work.

Another notable feature of the slipline theory is that we may build solutions for very large values of  $B$ . This is surprising in view of the idea that a rectangular (or triangular) block of material may not deform at all when released if its yield stress is sufficiently high. In this context, our results can be explained by the fact that the slipline construction gives an admissible stress field for a given volume of fluid. But there may be other admissible stress configurations, and which one of these configurations ultimately results depends on the initial condition and flow path. Hence, in an experiment that begins with a rectangular profile and large  $B$ , we may not be able to “reach” the solution constructed by the sliplines.

Pertaining to this, some work has been done to study the incipient failure of a rectangular block of viscoplastic material [1,17,18]. Pashias et al. [1] used a uniform stress model to predict that  $B \leq 1/2$  for slumping to occur. Chamberlain et al. [17], on the other hand, used plasticity theory and a slipline construction to show that the criterion for failure depends on the aspect ratio of the block, with critical values of  $B$  over the range 0.5–1.

In this paper we have studied two-dimensional deposits. We also attempted to apply the theory to axisymmetric slumps. However, this leads to several problems. In the general slipline problem, along with Eqs. (1)–(5), there are also the velocity equations (see, for example [9]). In two dimensions, the equations for the stress decouple from the velocity equations, and given suitable stress boundary conditions, the stresses can be determined independently, as we have done here. In the axisymmetric case, with an additional non-trivial component of stress, the stress equations no longer decouple, and the velocity field must be solved simultaneously with the stress field. One also needs an analogue of the expansion fan to begin the slipline construction, and suitable velocity boundary conditions on the free surface. One method which has been used to overcome some of these issues is the so-called Haar-Karman hypothesis [19,20], which assumes that the intermediate principal stress is equal to one of the other two principal stresses. Thus, one can eliminate one of the stress components from the stress equations, which then decouple from the velocity equations. However, with the Haar-Karman hypothesis, incompressibility is violated, a physical principle that we were reluctant to let go.

## Acknowledgements

ND would like to acknowledge the financial support of the Natural Sciences and Engineering Research Council of Canada. We thank Richard Craster and Stefan Llewellyn Smith for useful discussions.

## Appendix A. Shallow-layer perturbation equations

In this appendix we present the details of the asymptotic expansion of (10)–(15) for  $\epsilon \ll 1$ , assuming  $S$  is order one and that the maximal height  $h|_{x=0} = 1$ . We begin by expanding all variables except  $h$  in powers of  $\epsilon$  according to  $f = f_0 + \epsilon f_1 + \epsilon^2 f_2 + \dots$ . In order to avoid having to expand the boundary conditions (7) on the free surface as part of this first expansion, we assume  $h$  is known and drop the boundary condition on the base (15). Once  $\tau_{xz}$  is obtained to the desired order, we impose this boundary condition and find an equation for  $h$ . That equation can then be solved by a second expansion in  $\epsilon$  to yield the required profiles.

At leading order in  $\epsilon$ , the governing equations, (10)–(12), become

$$-\frac{\partial p_0}{\partial x} + \frac{\partial \tau_{0xz}}{\partial z} + S = 0, \quad \frac{\partial p_0}{\partial z} + 1 = 0, \quad \tau_{0xx}^2 + \tau_{0xz}^2 = 1, \quad (\text{A.1})$$

subject to

$$\tau_{0xz} = 0 \quad \text{and} \quad p_0 = 0, \quad \text{on } z = h, \quad (\text{A.2})$$

with solution

$$p_0 = h - z, \quad \tau_{0xz} = v, \quad \tau_{0xx} = -\sqrt{1 - v^2}, \quad (\text{A.3})$$

where  $v(x, z) = (h_x - S)(z - h)$ .

At order  $\epsilon$ , the governing equations are

$$-\frac{\partial p_1}{\partial x} + \frac{\partial \tau_{0xx}}{\partial x} + \frac{\partial \tau_{1xz}}{\partial z} = 0, \quad \frac{\partial p_1}{\partial z} + \frac{\partial \tau_{0xx}}{\partial z} = 0, \quad (\text{A.4})$$

$$\tau_{0xx} \tau_{1xx} + \tau_{0xz} \tau_{1xz} = 0,$$

with boundary conditions

$$(p_1 - \tau_{0xx})h_x + \tau_{1xz} = 0 \quad \text{and} \quad p_1 + \tau_{0xx} = 0 \quad \text{on } z = h, \quad (\text{A.5})$$

and solution

$$p_1 = \sqrt{1 - v^2}, \quad \tau_{1xz} = \frac{\partial}{\partial x} \left( \frac{v\sqrt{1 - v^2} + \sin^{-1} v}{h_x - S} \right), \quad (\text{A.6})$$

$$\tau_{1xx} = \frac{v}{\sqrt{1 - v^2}} \tau_{1xz}.$$

Finally, at order  $\epsilon^2$ , we have

$$-\frac{\partial p_2}{\partial x} + \frac{\partial \tau_{1xx}}{\partial x} + \frac{\partial \tau_{2xz}}{\partial z} = 0, \quad -\frac{\partial p_2}{\partial z} + \frac{\partial \tau_{0xz}}{\partial x} - \frac{\partial \tau_{1xx}}{\partial z} = 0, \quad (\text{A.7})$$

with

$$(p_2 - \tau_{1xx})h_x + \tau_{2xz} = 0 \quad \text{and} \quad p_2 + \tau_{1xx} + h_x \tau_{0xz} = 0 \quad \text{on } z = h, \quad (\text{A.8})$$

yielding

$$p_2 = \frac{\partial}{\partial x} \left[ \frac{v^2}{2(h_x - S)} \right] - \frac{v}{\sqrt{1 - v^2}} \frac{\partial}{\partial x} \left( \frac{v\sqrt{1 - v^2} + \sin^{-1} v}{h_x - S} \right), \quad (\text{A.9})$$

$$\tau_{2xz} = 2 \frac{\partial}{\partial x} \left[ \frac{h_{xx}}{(h_x - S)^3} (v - \sqrt{1 - v^2} \sin^{-1} v) \right] - \frac{1}{2} \frac{\partial^2}{\partial x^2} \left[ \frac{v^3}{(h_x - S)^2} \right]. \quad (\text{A.10})$$

Note that in (A.7) we have omitted the order  $\epsilon^2$  equation derived from (12) as it is not required for the solutions (A.9) and (A.10).

Imposing the basal boundary condition we now find

$$1 = V + \epsilon \frac{\partial}{\partial x} \left( \frac{V\sqrt{1 - V^2} + \sin^{-1} V}{h_x - S} \right) + \epsilon^2 \left( 2 \frac{\partial}{\partial x} \left[ \frac{h_{xx}}{(h_x - S)^3} (V - \sqrt{1 - V^2} \sin^{-1} V) \right] - \frac{1}{2} \frac{\partial^2}{\partial x^2} \left[ \frac{V^3}{(h_x - S)^2} \right] \right) + O(\epsilon^3), \quad (\text{A.11})$$

where  $V = v(x, 0) = -(h_x - S)h$ . Expanding  $h = h_0 + \epsilon h_1 + \epsilon^2 h_2 + \dots$  and setting  $h|_{x=0} = 1$ , we can then find the expressions for the slump profiles.

For a horizontal surface ( $S = 0$ ), we obtain

$$h = h_0 + \epsilon \frac{\pi}{2} \left( \frac{1}{h_0} - 1 \right) + \epsilon^2 \frac{\pi^2}{8h_0} \left( 1 - \frac{1}{h_0^2} \right) + O(\epsilon^3), \quad (\text{A.12})$$

where  $h_0 = \sqrt{1 - 2x}$ . Unfortunately, because  $h_0 \rightarrow 0$  as  $x \rightarrow 1/2$ , this asymptotic sequence becomes disordered for  $x - 1/2 \sim \epsilon^2$ . The singularity at  $x = 1/2$  can be removed to improve the uniformity of the asymptotic series by shifting the leading edge of the slump, as in the method of strained coordinates [21]. Alternatively, we can recognize the divergent terms in (A.12) as the Taylor series expansion of  $h_0$  about an edge that is shifted by an order  $\epsilon$  distance from  $x = 1/2$ . This observation leads us to regroup the divergent terms into the non-singular solution (19) quoted in Section 3 (which can also be derived directly using the method of strained coordinates).

For  $S \neq 0$ , the expansion of (A.11) furnishes the solution,

$$h = h_0 + \epsilon \frac{\pi}{2S} \frac{1 - Sh_0}{h_0} \mathcal{L} + \epsilon^2 \left[ \left( 3 - \frac{\pi^2}{4} \right) \frac{1 - Sh_0}{h_0} \mathcal{L} - \frac{\pi^2}{8S^2} \frac{1 - Sh_0}{h_0^3} \mathcal{L}^2 - \frac{\pi^2}{4S} \frac{1 - Sh_0}{h_0^2} \mathcal{L} \right] + O(\epsilon^3), \quad (\text{A.13})$$

where  $\mathcal{L}(S, h_0) = \log(1 - Sh_0) - \log(1 - S)$  and  $h_0(x)$  is given implicitly by  $h_0 - 1 + \mathcal{L}/S = Sx$ . This expansion again becomes disordered as  $x \rightarrow -\log(1 - S)/S^2 - 1/S$  and  $h_0 \rightarrow 0$ . Once more, we recognize the divergent terms as the Taylor series expansion of  $h_0$  and reformulate the solution in the non-singular fashion of (22).

## Appendix B. Calculation of the slipline field

The following calculations make reference to the slipline field sketched in Fig. 1. Note that in practice, however, the initial arc from the expansion fan ( $BE$  in Fig. 1) is partitioned into 160 intervals. Doubling the partition size to 320 resulted in negligible changes in the slipline field and the surface profile; the change was on the order of 0.01%.

### B.1. Surface point

Given, for example, the values  $x_B, z_B, P_B$ , and  $\theta_B$  and  $x_C, z_C, P_C$ , and  $\theta_C$  corresponding to the points  $B$  and  $C$ , respectively, from Eqs. (28) and (26) we obtain

$$P_F + 2\theta_F = P_C + 2\theta_B, \quad (\text{B.1})$$

$$P_F - z_F + x_F S - 1 = 0. \quad (\text{B.2})$$

We can also write first order expressions for the slopes of  $BF$  and  $CF$ :

$$z_F - z_B = (x_F - x_B) \tan \left( \frac{1}{2}(\theta_F + \theta_B) - \frac{\pi}{4} \right) \quad (\text{B.3})$$

$$z_F - z_C = (x_F - x_C) \tan \left( \frac{1}{2}(\theta_F + \theta_C) \right). \quad (\text{B.4})$$

In (B.3) we have implicitly used Eq. (30) (i.e., that the sliplines must intersect the surface at angle of  $\pm\pi/4$ ). Eqs. (B.1)–(B.4) are then solved to obtain  $x_F, z_F, P_F$ , and  $\theta_F$ .

### B.2. Interior point

Given, for example, the values  $x_F, z_F, P_F$ , and  $\theta_F$  and  $x_D, z_D, P_D$ , and  $\theta_D$  corresponding to the points  $F$  and  $D$ , respectively, we can then calculate the values  $x_G, z_G, P_G$ , and  $\theta_G$ . From (28) and (29) we obtain

$$P_G + 2\theta_G = P_D + 2\theta_D, \quad (\text{B.5})$$

$$P_G - 2\theta_G = P_F - 2\theta_F. \quad (\text{B.6})$$

Also, the first order expression for the slopes of  $DG$  and  $FG$  are, respectively,

$$z_G - z_D = (x_G - x_D) \tan\left(\frac{1}{2}(\theta_G + \theta_D)\right) \quad (\text{B.7})$$

$$z_G - z_F = (x_G - x_F) \tan\left(\frac{1}{2}(\theta_G + \theta_F) - \frac{\pi}{2}\right). \quad (\text{B.8})$$

Eqs. (B.5) and (B.6) can be rearranged to obtain

$$P_G = \frac{1}{2}(P_D + P_F) + (\theta_D - \theta_F), \quad (\text{B.9})$$

$$\theta_G = \frac{1}{4}(P_D - P_F) + \frac{1}{2}(\theta_D + \theta_F). \quad (\text{B.10})$$

With  $\theta_G$  now known (B.7) and (B.8) can be solved for  $x_G$  and  $z_G$ :

$$x_G = \frac{1}{T^* - T}(z_D - z_F + T^*x_F - Tx_D), \quad (\text{B.11})$$

$$z_G = \frac{1}{T^* - T}(T^*z_D - Tz_F + T^*Tx_F - T^*Tx_D), \quad (\text{B.12})$$

where

$$T = \tan\left(\frac{1}{2}(\theta_G + \theta_D)\right), \quad \text{and} \quad T^* = \tan\left(\frac{1}{2}(\theta_G + \theta_F) - \frac{\pi}{2}\right). \quad (\text{B.13})$$

### B.3. Base point

At a base point we must have  $z = 0$  and  $\theta = 0$ . Furthermore, given, for example,  $x_I$ ,  $z_I$ ,  $P_I$ , and  $\theta_I$  we may write

$$P_j - 2\theta_j = P_I - 2\theta_I \quad (\text{B.14})$$

$$z_j - z_I = (x_j - x_I) \tan\left(\frac{1}{2}(\theta_j + \theta_I) - \frac{\pi}{2}\right). \quad (\text{B.15})$$

Combining these conditions we can then write

$$P_j = P_I - 2\theta_I, \quad (\text{B.16})$$

$$\theta_j = 0, \quad (\text{B.17})$$

$$x_j = x_I - \frac{z_I}{\tan\left(\frac{1}{2}\theta_I - \frac{\pi}{2}\right)}, \quad (\text{B.18})$$

$$z_j = 0. \quad (\text{B.19})$$

### References

- [1] N. Pashias, D.V. Boger, J. Summers, D.J. Glenister, A fifty cent rheometer for yield stress measurement, *J. Rheol.* 40 (6) (1996) 1179–1189.
- [2] W.R. Schowalter, G. Christensen, Toward a rationalization of the slump test for fresh concrete: comparisons of calculations and experiments, *J. Rheol.* 42 (4) (1998) 865–870.
- [3] N. Roussel, P. Coussot, “Fifty-cent rheometer” for yield stress measurements: from slump to spreading flow, *J. Rheol.* 49 (3) (2005) 705–718.
- [4] P. Coussot, S. Proust, C. Ancey, Rheological interpretation of deposits of yield stress fluids, *J. Non-Newtonian Fluid Mech.* 66 (1996) 55–70.
- [5] S. Blake, Viscoplastic models of lava domes, in: J.H. Fink (Ed.), *Lava Flows and Domes: Emplacement Mechanisms and Hazard Implications*, IAVCEI Proceedings in Volcanology, vol. 2, Springer-Verlag, 1990, pp. 88–126.
- [6] R.W. Griffiths, The dynamics of lava flows, *Annu. Rev. Fluid Mech.* 32 (2000) 477–518.
- [7] N.J. Balmforth, R.V. Craster, A.C. Rust, R. Sassi, Viscoplastic flow over an inclined surface, *J. Non-Newtonian Fluid Mech.* 142 (2007) 219–243.
- [8] J.F. Nye, Plasticity solution for a glacier snout, *J. Glaciol.* 6 (47) (1967) 695–715.
- [9] R. Hill, *The Mathematical Theory of Plasticity*, Clarendon Press, Oxford, 1950.
- [10] J. Chakrabarty, *Theory of Plasticity*, Elsevier, Oxford, 2006.
- [11] N.J. Balmforth, R.V. Craster, R. Sassi, Shallow viscoplastic flow in an inclined plane, *J. Fluid Mech.* 470 (2002) 1–29.
- [12] S. Cochard, Measurements of time-dependent free-surface viscoplastic flows down steep slopes, PhD Thesis, École Polytechnique Fédérale de Lausanne, 2007.
- [13] C. Ancey and S. Cochard, The dam-break problem for Herschel–Bulkley viscoplastic fluids down steep flumes. *J. Non-Newtonian Fluid. Mech.*, this issue, doi:10.1016/j.jnnfm.2008.08.008.
- [14] J.F. Nye, The flow of glaciers and ice-sheets as a problem in plasticity, *Proc. R. Soc. Lond. Ser. A* 207 (1091) (1951) 554–572.
- [15] K.F. Liu, C.C. Mei, Slow spreading of a sheet of Bingham fluid on an inclined plane, *J. Fluid Mech.* 207 (1989) 505–529.
- [16] H. Chanson, P. Coussot, S. Jarny, and L. Toquer, A study of dam break wave of thixotropic fluid: Bentonite surges down an inclined plane, Technical Report CH 54/04, University of Queensland, 2004.
- [17] J.A. Chamberlain, J.E. Sader, K.A. Landman, L.R. White, Incipient plane-strain failure of a rectangular block under gravity, *Int. J. Mech. Sci.* 43 (2001) 793–815.
- [18] J.A. Chamberlain, D.J. Horrobin, K.A. Landman, J.E. Sader, Upper and lower bounds for incipient failure in a body under gravitational loading, *J. Appl. Mech.* 71 (2004) 586–589.
- [19] R.M. Nedderman, *Statics and Kinematics of Granular Materials*, Cambridge University Press, Cambridge, 1997.
- [20] J.A. Chamberlain, J.E. Sader, K.A. Landman, D.J. Horrobin, L.R. White, Incipient failure of a circular cylinder under gravity, *Int. J. Mech. Sci.* 44 (2002) 1779–1800.
- [21] M. Van Dyke, *Perturbation Methods in Fluid Mechanics*, Parabolic, Stanford, 1975.